 doi:10.20944/preprints202010.0498.v1

Optimal synthesis and mechanistic performance of HCO-doped-(Fe_3O_4)x adsorbent for Sb(III)/Sb(V) removal from water

Renjian Deng[a]*, Jun Zhang[a], Xiaoliang Hu[a], Chuanqu Zhu[a], Fubing Xie[b], Mohammed Yaseen[c], Andrew Hursthouse[ac], Xing Zeng[a]

[a]*School of Civil Engineering, Hunan University of Science and Technology, Xiangtan 411201, China*

[b] *Hunan* Jing Yi environmental protection high tech Development Co Ltd , Xiangtan 411201, China

c School of Computing, Engineering & Physical Sciences, University of the West of Scotland, Paisley, PA1 2BE UK

**Corresponding author: deng800912@163.com, andrew.hursthouse@uws.ac.uk*

Jun Zhang:z931021j@163.com

Xiaoliang Hu: 343651218@qq.com

Chuanqu Zhu:wzh1@hnust.edu.cn

Fubing Xie: xiefubing@yphb.com.cn

Mohammed YASEEN:mohammed.yaseen@uws.ac.uk

Andrew Hursthouse:Andrew.hursthouse@uws.ac.uk

Xing Zeng :526244285@qq.com

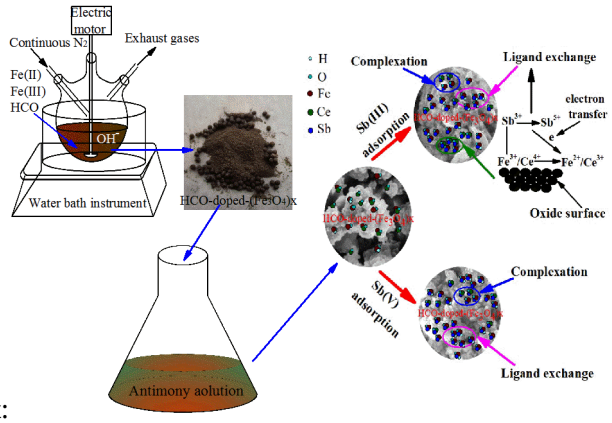

Graphical Abstract:

Abstract:

Concern over potential antimony mediated toxicity from mining and smelting activities has instigated novel concepts toward removing aqueous antimony ions. The iron based adsorbent Fe_3O_4/HCO was found to be efficient for treating antimony-containing wastewater However, ineffective methodology for preparation limited its effective adsorption capacity and thus wider application. In this study, a new type of HCO-doped-(Fe_3O_4)$_x$ adsorbent was prepared by co-precipitation method for doping Fe_3O_4 into HCO sludge (HCO), thereby improving adsorption performance for Sb(III) and Sb(V) ions, with the maximum adsorbing capacity being 44.46 mg/g and 47.91 mg/g, respectively. According to the results of BET, SEM-EDS, XRD and XPS, it were confirmed that the FeOOH and X≡Fe-OH were formed during the preparation process, bring about the increased the surface area, thus resulting in further increase of surface area, hydroxyl groups and the net negative ionic charge. Moreover, the adsorption kinetics followed the pseudo-second-order kinetic model which indicated that adsorption process of Sb(III)/Sb(V) by HCO-doped-(Fe_3O_4)$_x$ adsorbent was controlled by

 doi:10.20944/preprints202010.0498.v1

chemical reaction. The main adsorption mechanism is that antimony ion and amorphous iron oxide X≡Fe-OH undergo coordination exchange reaction and complexation reaction with CeO_2 or Ce_2O_3. Furthermore, HCO-doped-$(Fe_3O_4)_x$ could adapt to wide pH and had stable adsorption ability after regeneration. The good adsorption performance of HCO-doped-$(Fe_3O_4)_x$ makes it a potential applications of adsorbent for removal of antimony.

Keywords: HCO-doped-$(Fe_3O_4)_x$ adsorbent, Sb(III) and Sb(V), Ce/Fe molar ratio, Adsorption mechanism

1. Introduction

Antimony (Sb), if present above a certain concentration within the environmental, is a toxic agent [1,2]. It is a global pollutant and listed as a priority for control by the world health organization (WHO) and United States Environment Agency (USEPA) [3,4]. China has one of the largest antimony deposits in the world and minining is continuing. Thus, antimony contamination of water bodies continues to worsen in China because of anthropogenic and natural source contributions such as weathering of rocks, antimony mining and smelting, as well as the extensive use of antimony products [5-7]. For instance, near Xikuangshan mines which is considered as the capital of antimony mining, the Sb concentration in natural water bodies was found to be 37~63 μg/L [6], resulting in one of the most serious eco-environment problems. Sb(III) and Sb(V) are the main oxidation states of Sb found within the natural environment, and the two valence states can inter-transform [4]. At present, there is a lack of understanding of the bio-geochemical cycle, the chemical behavior of antimony, and the lack of efficient treatment technology. Purification of water contaminated by Sb(III)/Sb(V) has thus become an urgent problem in such antimony mining environments of China [8,9].

For the last 20 years, various technologies to purify antimony metals from water such as flocculation [10], chemical precipitation [8], ion exchange [11], bioremediation [12] and adsorption [13]. Among them, adsorption has garnered a great deal of attention [1,8,14], due to its the advantages of low-cost and simplicity. Meanwhile, Fe_3O_4 as a promising absorbent for antimony-containing wastewater treatment, has the advantage of economy, affective over a wide range of pH and easy recovery. However, the main limitation is low adsorption capacity [15]. Therefore, the preparation of Fe-carrying adsorbents with high antimony removal efficiency and large adsorption capacity is a current research focus [1,9]. Recently, it has been found that Fe_3O_4 doped with manganese, zirconium, cerium or other metals can be prepared as bimetallic composite adsorbent with porous structure [16-19], so as to improve its adsorption capacity [4, 20-22], and retain the advantages of Fe_3O_4, such as deposition speed, easy recovery and recycling [23-26]. One of the most abundant rare earth metals , cerium ions

Preprints (www.preprints.org) | NOT PEER-REVIEWED | Posted: 23 October 2020 doi:10.20944/preprints202010.0498.v1

and CeO_2 aqueous can carry many high affinity surface hydroxyl groups [27] with cerium ions providing a more positive charge density on the surface of adsorbent, which is conducive to the adsorption and removal of oxyanions of Sb, As and Cr [22,28]. Therefore, cerium and its oxides have received much attention in recent years in purification of water contaminated by metal ion [29, 30]. For example, it has been found that pure cerium doped Fe_3O_4 magnetic adsorbent exhibited a good antimony adsorption performance in aqueous solution [4,27,31,32]. However, Cerium, being a rare strategic metal, thus its high price restricted its extensive use. Therefore, under the guidance of the thought of "resource recycling" and "treat waste with waste", Fe_3O_4/HCO adsorbent was prepared using the grinding sludge rich in cerium oxide (CeO_2. nH_2O, referred to as HCO) and Fe_3O_4 as raw material [14]. As is well known, the preparation process of adsorbent doped metals via modified co-precipitation method would have significant effects; such as increased amount of specific surface area, pore size, hydroxy content, as well as tunable surface charge and electronic properties. These factors can greatly enhance the adsorption capacity and performance. However, the optimum preparation conditions of doped Fe_3O_4 onto HCO have never reported [14], leading to unclear control of its synthesis. On the other hands, the Ce/Fe molar ratio was also found to be a key factor toward controling the specific surface area and pore size of adsorbent, although the optimum Ce/Fe molar ratio for adsorption of antimony is still unclear. In addition, antimony in natural water mainly exists in the form of Sb(V) [1,2]. The influencing factors and mechanism of Sb(V) removal by Fe_3O_4/HCO adsorption and the difference with removal of Sb(III) are also in not optimized [14].

In this work, a series of new HCO-doped-$(Fe_3O_4)_x$ adsorbent were synthesized by co-precipitation method using Fe_3O_4 doped into grinding sludge with HCO rich grinding sludge as the substrate ratio of precursors conditions. Evaluation of their aqueous Sb(III) and Sb(V) sorption capacity, as well as the effect of Ce/Fe molar ratio, pH and reaction time on adsorption were investigated. Moreover, the adsorption isothermal model and adsorption kinetics model of Sb(III)/Sb(V) adsorbed by HCO-doped-$(Fe_3O_4)_x$ were constructed. Also the surface morphology, crystal structure, valence state of Sb(III)/Sb(V) before and after adsorption were investigated, as well as the possible adsorption removal mechanism further evaluated.

2. Materials and methods

2.1. Preparation and characterization of HCO-doped-$(Fe_3O_4)_x$

The raw HCO was collected from the LSKJ Co., Ltd sewage treatment plant. The major chemical ingredients of the raw HCO in addition to water (80.5%) are cerium oxide (7.8%),

Preprints (www.preprints.org) | NOT PEER-REVIEWED | Posted: 23 October 2020 doi:10.20944/preprints202010.0498.v1

silicon dioxide (4.5%), aluminium oxide (3.8%), calcium oxide (2.8%) and other material (0.6%). Taking a certain amount of HCO, dehydrated and dried it at 100 ℃, ground and then sieved through 100 mesh for standby.

HCO-doped-$(Fe_3O_4)_x$ adsorbents were prepared by modified co-precipitation method [14,33]. Firstly, dry sludge containing 0.1mol, 0.2mol and 0.3mol HCO was added into three 500-ml three-necked flask, respectively. Then 50ml of $FeSO_4.7H_2O$ (0.020 mol) and 50 ml of $FeCl_3.6H_2O$ (0.040 mol) solution was added under nitrogen atmosphere. Secondly, 200 ml of 7% ammonia solution was slowly added into the reactant mixture with stirring at 60 ℃ within water bath . Then, the reaction was carried out under nitrogen atmosphere for 2 hours to obtain a solution suspension. It was washed with deionized water and anhydrous ethanol, and then dried it at 80℃. Finally, the materials obtained were ground into a powder and stored for future use. HCO-doped-$(Fe_3O_4)_x$ adsorbents(x=0.5, 1.0 and 1.5,respectivly) were obtained. During the preparation, the possible chemical reactions were described as follows (Eq. (1-7)) [4,14,31].

$$Fe^{3+}+3OH^- \rightarrow Fe(OH)_3 \quad (1)$$

$$Fe^{2+}+2OH^- \rightarrow Fe(OH)_2 \quad (2)$$

$$2Fe(OH)_3+ Fe(OH)_2 \rightarrow Fe_3O_4+4H_2O \quad (3)$$

$$CeO_2.nH_2O+ 2xFe(OH)_3+ xFe(OH)_2 \rightarrow CeO_2\text{-doped-}(Fe_3O_4)_x+H_2O \quad (4)$$

$$Ce_2O_3.nH_2O+2xFe(OH)_3+ xFe(OH)_2 \rightarrow Ce_2O_3\text{-doped-}(Fe_3O_4)_x+H_2O \quad (5)$$

$$Fe_3O_4+ 6CeO_2.nH_2O +OH^- = 3FeCe_2O_4\downarrow+3H_2O \quad (6)$$

For your convenience, the Eq.(4) and Eq.(5) are written as Eq.(7).

$$HCO+2xFe(OH)_3+ xFe(OH)_2 \rightarrow HCO\text{-doped-}(Fe_3O_4)_x+H_2O \quad (7)$$

The textural properties of HCO, HCO-doped-$(Fe_3O_4)_x$ and after Sb adsorption were characterized by SEM-EDS (Bruker XFlash 5010, Germany) spectrometer at the desired magnification. The compounds in HCO-doped-$(Fe_3O_4)_x$ before and after preparation and after Sb adsorption were analyzed by X-ray diffractometer (XRD,D8 Advance, Brook AXS Ltd.,Germany) under the condition of scanning range of 10-90°at 40 mA and 40 Kv, with a scan rate of 1°/min^{-1} and step size of 0.02°. The valence states of Ce, Fe and Sb in HCO-doped-$(Fe_3O_4)_x$ samples before and after adsorption were analyzed by X-ray electron spectroscopy (XPS, Thermo Scientific: Esala 250Xi) to determine their binding states. All binding energies (B.E.) are based on the carbon peak C1s at 285.1ev, and the analysis software is XPS peak [4,14]. The Brunauer-Emmett-Teller (BET) surface areas of the adsorbents were determined by nitrogen adsorption/desorption isotherms using Anton Paar GmbH analyzer (Quantachrome Instruments, version, Autosorb EVO, USA).

Preprints (www.preprints.org) | NOT PEER-REVIEWED | Posted: 23 October 2020 doi:10.20944/preprints202010.0498.v1

2.2 Adsorption and desorption experiments

The effect of Ce/Fe molar ratio, pH and reaction time, adsorption isotherm and kinetics were carried out in batch adsorption experiments. Desorption experiments were executed to investigate the reusability and regeneration potential of the sorbent [4].

2.2.1 Adsorption experiments

For the effect of Ce/Fe molar ratio, five 100 ml solutions were prepared with an initial Sb(III)/Sb(V) concentration of 20 mg/L. The solution pH was adjusted to 5 ± 0.1 by 1 mol/L HCl or 1 mol/L NaOH. Then, 0.2g HCO-doped-$(Fe_3O_4)_x$ adsorbents, which x=1:0, 0:1, 0.5, 1, 1.5, respectively, were added into the solution. Adsorption was conducted at the temperature of 25±1℃ and a stirring rate of 150 r/min. Under equilibrium adsorption, about 5 ml aliquots were filtered by using 0.45μm membrane and the residual concentration of Sb(III)/Sb(V) determined. Then, the removal rate and adsorption capacity were calculated. All trials were repeated three times. According to the removal rate and adsorption capacity of Sb(III) and Sb(V), the best Ce/Fe molar ratio of HCO-doped-$(Fe_3O_4)_x$ adsorbents were selected for subsequent test.

Effect of pH on removal of Sb(III)/Sb(V) was also investigated. An aliquot of Sb(III)/Sb(V) stock solution was added to triangular bottle, and the volume was increased to 100 mL with distilled water to obtained initial Sb(III)/Sb(V) concentration of 20 mg/L. Then, the solution pH was adjusted to the given values (2.0-9.0) by 1 mol/L HCl or 1 mol/L NaOH, 0.2 g HCO-doped-$(Fe_3O_4)_x$ (x=1 or 1.5) adsorbents were added in triangular bottle and shaken at 150 r/min for 2 hours at the temperature of 25±1℃. The concentration of Sb(III)/Sb(V) after equilibrium adsorption was determined.

To investigate the influence of reaction time on the removal of Sb(III)/Sb(V), 0.2 g HCO-doped-$(Fe_3O_4)_x$ (x=1.0 or 1.5) adsorbents were added into 100 ml solution with the initial Sb(III)/Sb(V) concentration of 20 mg/L and initial pH of 5, then about 4 mL aliquots were taken from the suspension at predictable times (30 min-12 h) for measuring the remaining Sb(III)/Sb(V) concentration.

2.2.2 Adsorption isothermal experiment

For adsorption isothermal experiment, 0.2g HCO-doped-$(Fe_3O_4)_x$ adsorbents were added into triangular bottle and then made up to 100 ml with concentration gradient of (10-200 mg/L for Sb(III)) and (10-100 mg/L for Sb(V)) [34], respectively. The pH of solution was maintained at pH 5.0 using 0.1 mol/L HCl or 0.1 mol/L NaOH with shaking at 150 r/min for 6 h at the temperature of 25±1℃. After filtration with 0.45 μm membrane, the residual concentration of Sb(III)/Sb(V) was measured. The adsorption isotherm models, such as Langmuir and Freundlich [8,9,14], were used to fit the experimental data. The model formulas

Preprints (www.preprints.org) | NOT PEER-REVIEWED | Posted: 23 October 2020 doi:10.20944/preprints202010.0498.v1

of Langmuir and Freundlich models are shown in Eq. (8) and Eq. (9), respectively.

$$\frac{C_e}{q_e} = \frac{1}{q_{\max} b} + \frac{C_e}{q_{\max}} \tag{8}$$

$$\lg(q_e) = \lg(K_f) + \frac{1}{n}\lg(C_e) \tag{9}$$

Where, C_e (mg/L) is the concentration of Sb(III)/Sb(V) in the solution at adsorption equilibrium, q_e (mg/g) and q_{max} (mg/g) are equilibrium adsorption capacity and maximum adsorption capacity respectively, b (L/mg) is the adsorption constant of Langmuir, K_f and $1/n$ are the constants of Freundlich.

2.2.3 Adsorption kinetics experiment

According to the experimental results in section 2.2.1, adsorption kinetics experiments carried out to a 100 ml solution of Sb(III)/Sb(V) of 100 mg/L, 0.2g of HCO-doped-$(Fe_3O_4)_x$ adsorbent was added and shaken at a constant temperature of 25 ℃. The supernatant was taken off at different reaction time and filtered through 0.45 um membrane. The residual concentration of Sb, the removal rate and the adsorption capacity of Sb was calculated. The data were fitted by the Pseudo-first-order and Pseudo-second -order kinetic models [8,9,14]. The model formulas are shown in Eq. (10) and Eq. (11), respectively.

$$q_t = q_e(1 - \exp(k_1 t)) \tag{10}$$

$$q_t = q_e - q_e(k_2 q_e t + 1) \tag{11}$$

Where, t (min) is adsorption time, q_t (mg/g) and q_e (mg/g) are the adsorption quantity at time t and the adsorption equilibrium, respectively. k_1 (min^{-1}) is the adsorption rate constant of Pseudo-first-order kinetic models, k_2 (g/(mg·min)) is the adsorption rate constant of the Pseudo-second-order kinetic models.

2.2.4 Desorption experiment

In order to evaluate regeneration performance of this adsorbents, Sb(III)/Sb(V) of HCO-doped-$(Fe_3O_4)_x$ adsorbents were desorbed and adsorbed with 0.1mol/L NaOH solution according to the reports in the literature [4,14]. After filtration and drying, the regenerated adsorbents were reused to evaluate recycle ability.

2.3 Analysis method

The standard stock solution of Sb(III)/Sb(V) of 1.0 g/L was prepared with antimony potassium tartrate and potassium pyroantimonate [14,18]. Appropriate amount of stock solution was taken and diluted to obtain the required concentration of Sb(III)/Sb(V) solution. All reagents used in the experiment were analytical pure or superior pure, and the

Preprints (www.preprints.org) | NOT PEER-REVIEWED | Posted: 23 October 2020 doi:10.20944/preprints202010.0498.v1

experimental water was deionized water.

Determination of Sb(III)/Sb(V) in solution by Hydride Generation Atomic Fluorescence Spectrometry(AF-9600, Beijing Kechuang Haiguang Instrument Corporation, China) [14]. The test analysis was completed within 24h after the experiments, and the blank test was conducted with deionized water. With this method the minimum detection concentration is 1 μg/L, and antimony recovery at more than 90% within 1% error.

3 Results and discussion

3.1 Characterization analysis

The apparent morphology characteristics of HCO sludge and HCO-doped-$(Fe_3O_4)_x$ adsorbents (x=0.5,1 and 1.5) are shown in Fig. 1. The surface of HCO sludge exhibited a smoother surface typical of less-pores structure (Fig. 1(a)). After doping Fe_3O_4, more crystaline particles, typical of more-porous structure appeared on the surface of the adsorbent (Fig. 1 (b, c, d)). Moreover, the surface roughness porosity increased with the increase of Ce/Fe molar ratio (Table 1). The EDS energy spectrum (Fig. S1, and Table S1) showed that the main chemical components of HCO sludge were Ce (31.92%) and O (27.26%). The main chemical components of HCO-doped-$(Fe_3O_4)_x$ were Fe (28.49-16.07%), Ce (27.64-13.85%) and O(17.28-26.51%). The actual ratio Ce/Fe molar ratios were 0.49, 1.14 and 1.72, respectively, which were very close to the design values. The results indicated that Fe was successfully doped into HCO sludge by the improved co-precipitation method [4], and the adsorbents with porous and multi-active sites had been formed.

The porous characteristics of the adsorbents were confirmed by the S_{BET} parameters which were measured by nitrogen adsorption-desorption measurements (Table 1). As shown in Table 1, the S_{BET} was found to be 98.64 m^2/g for the sample of HCO-doped-$(Fe_3O_4)_{0.5}$, and it was 2.4 times higher than the value of HCO sludge sample (40.60 m^2/g). Moreover, when the Ce/Fe molar ratio increased from 0.5 to 1.5, both of the S_{BET} value (from 98.64 m^2/g to 108.57 m^2/g) and he total pore volume (V_{tot}) (0.159 cm^3/g to 0.224 m^3/g) increased, but the average pore diameter (6.77nm to 4.82 nm) decreased a similar result also can be found from cerium doped Fe_3O_4 by Qi et al [4]. It can be inferred that increase of Ce/Fe molar ratio could provide more active sites for diffusion and adsorption [4,35], which was consistent with the conclusion of Qi et al. [4]. We attempted to improve the Ce/Fe molar ratio to more than 1.5, but adsorbents with more-porous structure weren't formed. The reason for this outburst was still uncertain, and expected to be further researched.

The HCO sludge and as-prepared HCO-doped-$(Fe_3O_4)_x$ were characterized using XRD to identify the phases present (Fig.2(a)). From the diffraction pattern, it was suggested that all

Preprints (www.preprints.org) | NOT PEER-REVIEWED | Posted: 23 October 2020 doi:10.20944/preprints202010.0498.v1

the space group could be indexed in the cubic Fd3m comparing data with PDF-4+. As shown in Fig.2(a),there were 9 main peaks at 2θ= 28.50 °, 33.03 °, 47.46 °, 56.32 °, 59.07 °, 69.42 °, 76.71 °, 79.11 ° and 88.38 °, belonging to (111), (200), (220), (311), (222), (400), (331), (420) and (422) Cerianite crystal faces [36], respectively. However, in HCO-doped-$(Fe_3O_4)_x$ adsorbents, the intensity of the Cerianite character diffraction peak decreased and the position of character diffraction peak changed, suggesting that Fe doping changed the crystal structure of Cerianite [4,28], and formed a lot of multi-pore adsorbents. Combined with the analysis of XPS peak software, the results implied that the compound reaction between Fe_3O_4 and HCO occurred in the preparation process (Eq. (6)), and formed $FeCe_2O_4$ which was favorable for antimony adsorption [4, 14].

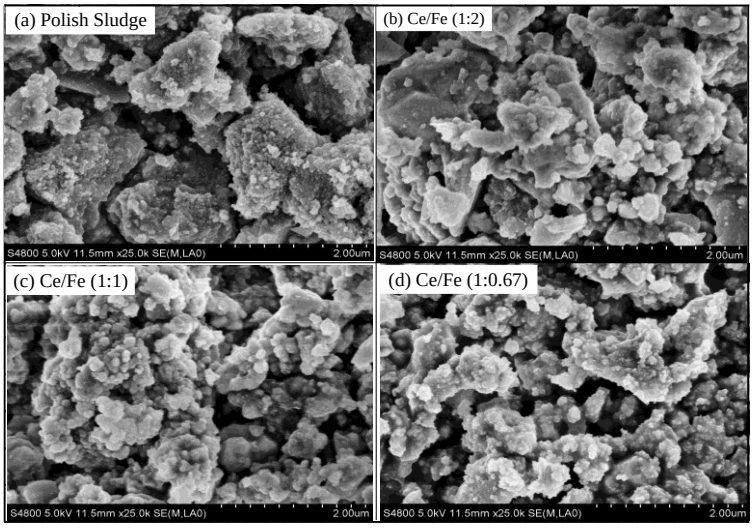

Fig. 1 SEM comparison of HCO-doped-$(Fe_3O_4)_x$ adsorbent

Table 1 characterization parameters of the different HCO-doped-$(Fe_3O_4)_x$ adsorbents

Parameters	Kinds of adsorbents			
	HCO sludge	HCO-doped-$(Fe_3O_4)_{0.5}$	HCO-doped-$(Fe_3O_4)_{1.0}$	HCO-doped-$(Fe_3O_4)_{1.5}$
Ce/Fe ratios	1:0	1:2=0.5	1:1=1.0	1:0.67=1.5
O(wt%)	27.26	17.28	26.51	26.15
Ce(wt%)	31.92	13.85	23.09	27.64
Fe(wt%)	0.64	28.49	21.82	17.56
$S_{BET}(m^2/g)$	40.60	98.64	105.12	108.57
$V_{tot}(cm^3/g)$	0.109	0.159	0.214	0.228
Average pore diameter（nm）	17.46	6.77	5.53	4.82
Actual Ce/Fe ratios	0.0	0.49	1.06	1.57

Note: $S_{BET:}$ the Brunauer-Emmett-Teller (BET) surface areas, m^2/g; $V_{tot:}$ the total pore volume, Actual ratio Ce/Fe= Ce(wt%)/Fe(wt%).

The full scan XPS spectrum for all kinds of HCO adsorbent exhibited in Fig.2 (b). The

Preprints (www.preprints.org) | NOT PEER-REVIEWED | Posted: 23 October 2020 doi:10.20944/preprints202010.0498.v1

results showed that the main components of HCO sludge and HCO-doped-$(Fe_3O_4)_x$ adsorbent were O and Ce, which was consistent with EDS analysis results (Fig.S1). Moreover, new peaks corresponding to Fe were detected in Fe containing HCO-doped-$(Fe_3O_4)_x$ adsorbents, indicating that Fe was successfully loaded in HCO sludge.

There were two strong diffraction peaks at the binding energies of 711ev and 724ev (Fig. 2(c)), and previous studies have shown that Fe at 711ev was mainly in the form of FeOOH and Fe_3O_4, and at 724ev was mainly in the form of Fe_2O_3 [4]. Therefore, it was inferred that Fe mainly existed in forms of three states of matter: FeOOH, Fe_3O_4 and Fe_2O_3 [4,27,31,32]. Fortunately, the three amorphous iron oxides showed excellent antimony removal properties [16,37,38], implying doping Fe in HCO sludge achieves the expected purpose. XPS scanning could be applied to verify the sample on account of its sensitivity to Sb(III)/Sb(V) and Fe^{2+}/Fe^{3+} ions. Fig. 2(d) shows the Ce3d narrow-scan spectra for HCO-doped-$(Fe_3O_4)_x$ adsorbents sample. The HCO-doped-$(Fe_3O_4)_x$ doublet consisted of four wide peaks of Ce $2p_{3/2}$ (882.00ev, 890.00ev and 900.00ev) and Ce $2p_{1/2}$ (916.00ev) [4,28], which were mainly ascribed to Ce-O bonds and the values are very close to those of cerium dioxide(CeO_2) and dicerium trioxide (Ce_2O_3) reported in the literatures [4,14]. So, we inferred that Ce^{3+} and Ce^{4+} were two valence states in HCO-doped-$(Fe_3O_4)_x$ adsorbent. The hydrolysis of cerium dioxide and dicerium trioxide ions can carry hydroxyl group [27], which could promote the removal and adsorption of antimony ions.

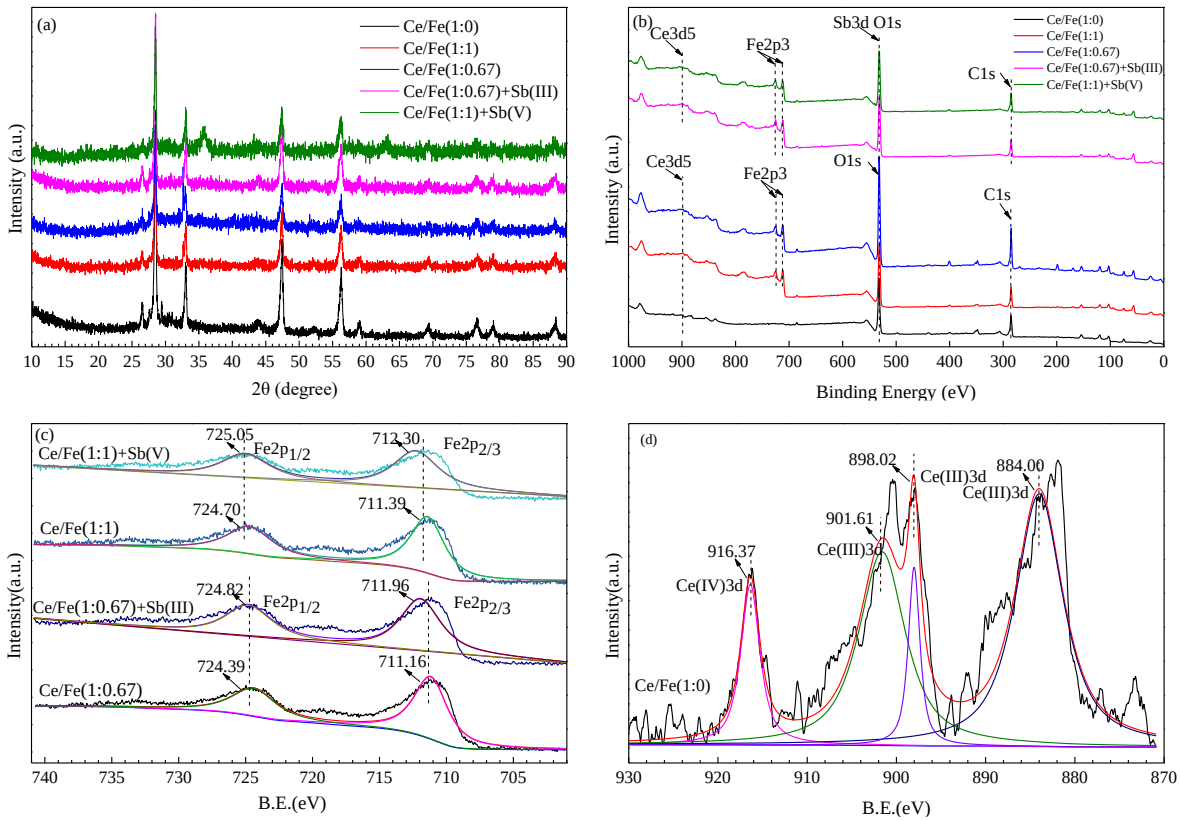

Preprints (www.preprints.org) | NOT PEER-REVIEWED | Posted: 23 October 2020 doi:10.20944/preprints202010.0498.v1

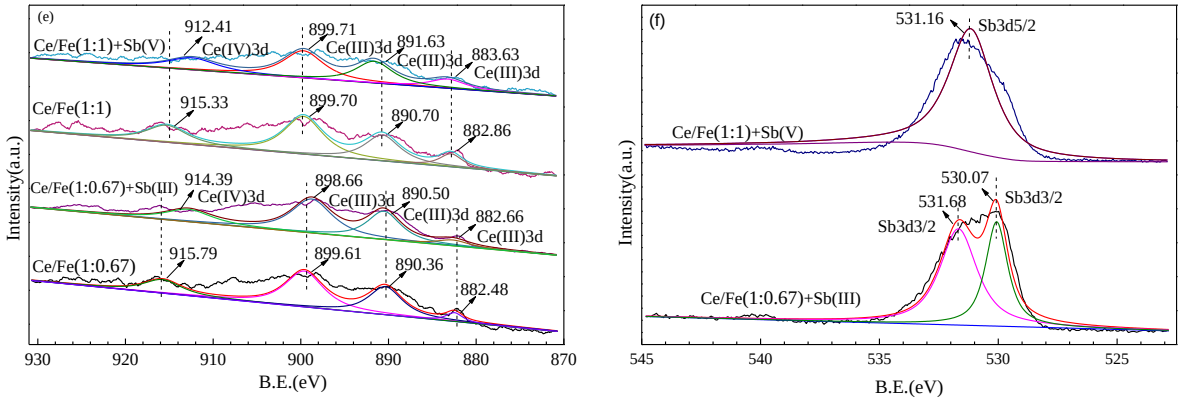

图 2 XRD (a) and XPS (b) before and after adsorption of Sb(III) and Sb(V) by HCO-doped-$(Fe_3O_4)_x$ adsorbent, and fine XPS analysis of Fe2p (c), Ce3d (d) (E) and Sb3d (f).

3.2 Effect of Ce/Fe molar ratio

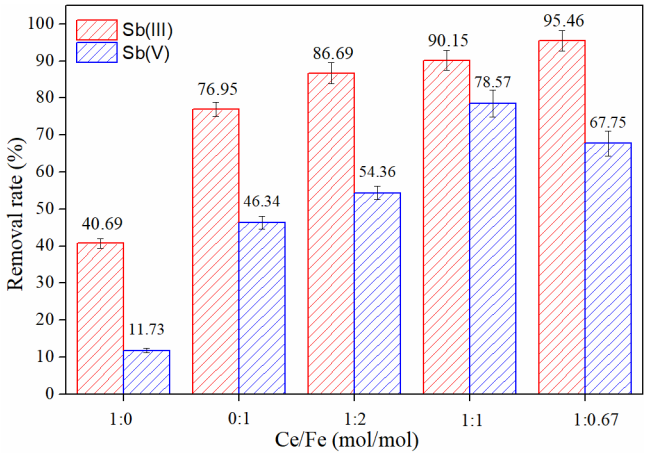

Fig. 3 Effect of Ce/Fe molar ratio on Sb(III)/Sb(V) removal by HCO-doped-$(Fe_3O_4)_x$ adsorbent: initial [Sb(III)]=[Sb(V)]=20 mg/L, adsorbents doses=2.0 g/L, pH=5.0±0.1

Fig.3 shows the effects on the Sb(III)/Sb(V) removal by different Ce/Fe adsorbent ratios. From comparision of HCO (Ce/Fe molar ratio=1:0) and Fe_3O_4 (Ce/Fe molar ratio=0:1), it is quite apparent that Fe_3O_4 is a better adsorbent than HCO. A further comparison of HCO (Ce/Fe molar ratio=1:0) and Fe_3O_4 (Ce/Fe molar ratio=0:1) with HCO-doped-$(Fe_3O_4)_x$ shows that the composite greatly improve the removal rate of Sb(III)/Sb(V), indicating that Fe_3O_4 doped in HCO is an effective way to remove the antimony ion from aqueous solution.

The results showed that the Sb(III) removal rate increasing from 86.69% to 95.46% with Ce/Fe molar ratio increasing from 0.5 to 1.5 (Fig.3). In addition, a positive correlation was found between Sb(III) removal rate and Ce/Fe molar ratio, which was absolutely consistent with other obtained results by Qi et al. [4,31]. However, with the increase of Ce/Fe molar ratio from 0.5 to 1.5, the Sb(V) removal rate first increased from 54.36% to 78.57%, then decreased to 67.75%, this also means there was not linear relationship between them. The results show optimum efficiency for removal of Sb(III) is when Ce/Fe molar ratio is 1.5, but

Preprints (www.preprints.org) | NOT PEER-REVIEWED | Posted: 23 October 2020 doi:10.20944/preprints202010.0498.v1

optimum for removal of Sb(v) is when Ce/Fe molar ratio is 1. Therefore, the removal characteristics of Sb(III) onto HCO-doped-$(Fe_3O_4)_x$ are much different from those of Sb(V). The reason might be due to the different reaction process between Sb(III) and Sb(V) with HCO-doped-$(Fe_3O_4)_x$. It is generally known that the hydroxyl group with high affinity carried by Ce_2O_3 play a major role in the process of adsorption and removal of Sb(III) [27]. Therefore, more hydroxyl group would be formed with the increase of Ce/Fe molar ratio, and corresponding Sb(III) removal rate increased. However, Sb(V) ions were mainly removed by the complexation of FeOOH and X≡Fe-OH [4, 28]. The higher concentration of HCO doped elements hampered the nucleation process of amorphous iron particles, and corresponding the structure and valence of amorphous iron (Fe_3O_4) were affected [4], thereby reducing the removal performance of Sb(V). In addition, the removal performance of Sb(III) by HCO-doped-$(Fe_3O_4)_x$ was significantly higher than those of Sb(V) under the same conditions. In conclusion, HCO-doped-$(Fe_3O_4)_{1.5}$ and HCO-doped-$(Fe_3O_4)_1$ had the best adsorption and removal effect on Sb(III) and Sb(V), respectively. Consequently, they were used for subsequent Sb(III) and Sb(V) adsorption and removal studies.

3.3 Effect of pH and adsorption time

The pH of the solution to be treated is an important factor affecting the adsorption capacity of the adsorbent [1,2]. The effect of different initial pH on Sb(III) and Sb(V) removal by HCO-doped-$(Fe_3O_4)_x$ adsorbent are shown in Fig.4(a). As can be seen, the removal rate of Sb(III) remained at a higher level (94.00-98.17%) with the pH value ranging from 2.0 to 7.0 after which there is a small reduction in removal rate efficiency toward pH9 as shown, Therefore, pH had very little effect on the adsorptive removal of Sb(III) by HCO-doped-$(Fe_3O_4)_{1.5}$, implying the adsorption of Sb(III) onto HCO-doped-$(Fe_3O_4)_{1.5}$ could adapt to wide pH value. In comparison, the removal rate of Sb(V) was at 94.91% at pH of 2.0, however it then descended to 48.87% at pH 9.0. The results indicated that pH significantly effects the adsorptive removal of Sb(V) by HCO-doped-$(Fe_3O_4)_{1.5}$, which was consistent with the conclusions of Qi and Deng et al [4, 8]. It was generally known that pH would determine the existence of Sb(III) and Sb(V) in aqueous solution [39], and also affect the degree of hydrolysis of amorphous iron such as FeOOH in HCO-doped-$(Fe_3O_4)_{1.5}$ [4]. Sb(III) mainly exists in the form of $Sb(OH)_3$ or H_3SbO_3 in the aqueous solution with the pH value ranging from 2.0 to 7.0 [4,39]. Both of $Sb(OH)_3$ and H_3SbO_3 can easy interact with Fe_3O_4 and Ce_2O_3 to form X≡Fe-$Sb(OH)_2$ precipitates [40] and $CeSbO_3$ [41] when the pH value of solution is between 2.0 to 7.0. Therefore, the removal rate of Sb(III) has been maintained in the higher level. But if pH continues to rise, FeOOH formation and iron ion dissolution would be inhibited [9], which would lead to the decrease of Sb(III) removal rate, alsoconsistent with the

Preprints (www.preprints.org) | NOT PEER-REVIEWED | Posted: 23 October 2020 doi:10.20944/preprints202010.0498.v1

research conclusion of Fan et al. [35]. As shown in Fig.3, at pH values higher than 2.0, Sb(V) adsorption decreased with further increase in the pH of the solution. The adsorption behavior can be explained in terms of the distribution of Sb(V) species. When the pH was 2-2.7, Sb(V) mainly exists in the form of H_3SbO_4 in the aqueous solution [4,39], which benefits the adsorption of antimony through substitution of hydroxyl ions coordinated with the metal ions loaded on the HCO-doped-$(Fe_3O_4)_{1.0}$. However, at pH values higher than 2.7, the concentration of $Sb(OH)_6^-$ increased with an increase in pH [4,39], and resulting in a decrease in Sb(V) adsorption through growing competition between OH^- and $Sb(OH)_6^-$ [35]. Overall, HCO-doped-(Fe_3O_4)x show better absorption capability at relatively wide range of pH in comparison with other iron containing or iron loaded composite adsorbents (Table 2) [37,42-45]. In conclusion, the optimal pH for HCO-doped-(Fe_3O_4)x adsorbing Sb(III) and Sb(V) should be controlled at 2-7 and 2-4, respectively.

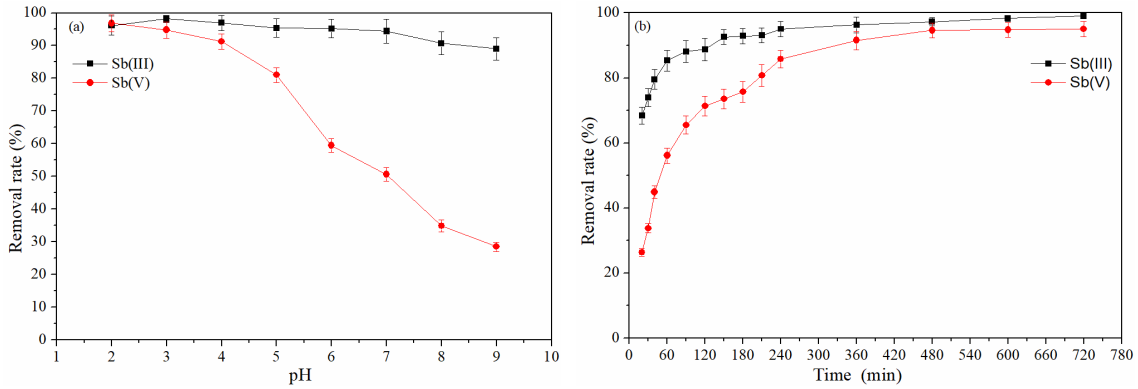

Fig.4 Effect of pH (a) and adsorption time (b) on Sb(III) and Sb(V) adsorption onto HCO-doped-$(Fe_3O_4)_x$ adsorbent (Initial concentration of Sb(III)]/Sb(V) =20mg/L, adsorbents doses=2.0g/L).

Adsorption equilibrium time is an important parameter to evaluate the performance of adsorbent. The results showed that the equilibrium time was about 4h and 8h (Fig.4 (b)), respectively, and indicated that adsorptive velocity of Sb(III) on HCO-doped-$(Fe_3O_4)_{1.5}$ was higher than that of Sb(V). The main reason for this was that the adsorption of Sb(III) on HCO-doped-$(Fe_3O_4)_{1.5}$ adsorbent belongs to monolayer adsorption [4,14] and the adsorption process of adjacent adsorption sites will not affect each other. HCO-doped-$(Fe_3O_4)_{1.0}$ adsorbent adsorption Sb(V) belongs to multilayer adsorption, and the adsorption speed is determined by the adsorption rate related to solution concentration and temperature [8], which is consistent with the conclusions of the subsequent adsorption isothermal model. It is noteworthy to mention that the time to achieve equilibrium was shorter for this composite than that of other iron associated composite adsorbents (Table.3). For example Fe/Mn bimetallic oxide (Sb(III)(5h)) [16], Fe/Zr loaded orange waste(Sb(III) and Sb(V)(24h)) [19], Fe_3O_4 loaded zeolite(Sb(V)(13h)) [46], and so on. Consequently, HCO-doped-(Fe_3O_4)x may

Preprints (www.preprints.org) | NOT PEER-REVIEWED | Posted: 23 October 2020 doi:10.20944/preprints202010.0498.v1

have wide application potential in the future.

3.4 Adsorption isothermal

The isotherm adsorption model, for which the definition and fitting accuracy are related to the type of adsorption materials, antimony ion valence, initial concentration, pH value and other factors [8,9,35], can reflect the relationship between adsorption capacity and solution concentration of adsorption materials at a specific temperature. The Sb(III)/Sb(V) adsorption capacities of the HCO-doped-$(Fe_3O_4)_x$ at pH 5.0 (25℃) were shown in Table 2. As shown in Table 2, the higher regression coefficient (R^2=0.98) implied that Langmuir model was suitable for representing the adsorption process of Sb(III) onto HCO-doped-$(Fe_3O_4)_{1.5}$. As is well known, the Langmuir model assume that all adsorption sites on the surface of adsorption matrix had the same solute affinity, and the adsorption process of adjacent adsorption sites would not affect each other [8,14,35]. We concluded that the adsorption of Sb(III) took place on the surface of HCO-doped-$(Fe_3O_4)_{1.5}$, which was defined as monolayer adsorption and chemical adsorption [8]. At the same time, the higher regression coefficient (R^2=0.945) implied that Freundlich model was suitable for describing the adsorption process of Sb(V) onto HCO-doped-$(Fe_3O_4)_{1.0,}$ which wasn't consistent with the conclusions of Qi et al [4,8]. In addition, we could make further inference that Sb(V) was most easily adsorbed by HCO-doped-$(Fe_3O_4)_{1.0}$ because of the parameter 1/*n* (0.486) less than 0.5. Also the adsorption process included single-layer (chemical) and multi-layer (physical) adsorption [8], belonging to synergistic adsorption [8,35]. Moreover, the value 1/*n* of Sb(III) from HCO-doped-$(Fe_3O_4)_{1.5}$ was smaller than that of Sb(V) with HCO-doped-$(Fe_3O_4)_{1.0}$, suggesting that Sb(III) was more easily adsorbed by HCO-doped-$(Fe_3O_4)_x$ composite adsorbent than Sb(V) [47]. The calculated maximum adsorption capacity for Sb(III) and Sb(V) was 44.46 mg/g and 47.91 mg/g, respectively, which demonstrated that it has good adsorption properties in comparison with other iron containing composite adsorbents (Table 3), such as $MnFe_2O_4$ adsorption Sb(III) (10.66 mg/g) [48], Fe_3O_4/HCO adsorption Sb(III) (22.85 mg/g) [14],Ce-doped magnetic biochar adsorption Sb(V) (25.0 mg/g) [28], Fe(III) modified fungal aerobic sludge adsorption Sb(V) (19 mg/g)) [49] and other ferric adsorbents. However, the maximum adsorption capacity in this study is smaller than those of other iron containing composite adsorbents (Table 3), Fe-Zr bimetallic oxide (60.4 mg/g) [44], Fe/Mn bimetallic oxide (214.28 mg/g) [16], Fe/Zr loaded orange waste (170.45-227.67 mg/g) [19], still provided some obvious advantages for practical aqueous removal of Sb(III)/Sb(V) because of achieving the concept of disposal waste with waste and recycling.

Table 2 Adsorption isotherm model parameters

Adsorbate	Langmuir	Freundlich

Preprints (www.preprints.org) | NOT PEER-REVIEWED | Posted: 23 October 2020 doi:10.20944/preprints202010.0498.v1

	q_{max}/(mg/g)	b/(L/mg)	R^2	K_f	1/n	R^2
Sb(III)	44.46	0.104	0.980	7.865	0.381	0.957
Sb(V)	47.91	0.108	0.757	7.273	0.486	0.946

Table 3 Comparison of adsorption properties of different adsorbents for Sb(III) and Sb(V)

Adsorbent	Adsorbate	Initial concentration (mg/L)	pH	React time (h)	Adsorption capacity (mg/g)	Removal rate (%)	Reference
Fe-Zr bimetallic oxide	Sb(V)	0-25	7	3	60.4	-	[44]
Hematite magnetic nanoparticles	Sb(III)	0.11	4.1	2	36.7	95.5	[43]
γ-FeOOH	Sb(V)	6.09	4	24	34.09	-	[37]
Nano FeOOH modified zeolite	Sb(III)	-	<2.7	-	7.17	-	[42]
Fe(III)-treated bacteria aerobic granules	Sb(V)	20	3.4	5	22.6	95	[45]
Fe/Mn bimetallic oxide	Sb(III)	24.35-234.5	3	5	214.28	-	[16]
Fe /Zr loaded orange waste	Sb(III)/ Sb(V)	15	2.5	24	170.45/227.67	-	[19]
Fe_3O_4 loaded zeolite	Sb(V)	5.1	2-4	13	19	85	[46]
Ce-doped magnetic biochar	Sb(V)	50	2-12	15	25.0	-	[28]
$MnFe_2O_4$	Sb(III)	894.3	2.0	-	10.66	-	[48]
Fe(III)-treated fungi aerobic granules	Sb(V)	20	3.4	5	19	-	[49]
Fe_3O_4/HCO adsorbent	Sb(III)	10-200	7.0	2	22.85	>90	[14]
HCO-doped-$(Fe_3O_4)_x$ adsorbent	Sb(III)	10-200	2-7	4	44.46	98.17	This study
	Sb(V)	10-100	2-4	6	47.91	81-96	

3.5 Adsorption kinetics

The adsorption kinetic model can describe the potential rate control and adsorption mechanism of material transport as well as chemical reaction in the adsorption process [14,35]. Calculated parameters on adsorption kinetics of Sb(III)/Sb(V) on HCO-doped-$(Fe_3O_4)_x$ are shown in Table 4. As seen in Table 4, the regression coefficient (R^2) showed suggested that the Sb(III)/Sb(V) adsorption kinetics could be better fitted by pseudo-second-order kinetic model. We inferred that electron sharing or electron transfer was the main source of adsorption power [14,28], and the adsorption process was controlled by the chemical reaction [14, 28]. Moreover, the calculated *qe* values (37.845 mg/g for Sb(III) and 44.029 mg/g for Sb(V)) were close to the experimental values (44.46 mg/g and 47.91 mg/g), which further implied that the whole adsorption process of Sb(III) and Sb(V) was controlled by the solid-liquid interface chemical reaction [35]. Furthermore, Elovich model also fitted well for the adsorption of Sb(III) and Sb(V) onto HCO-doped-$(Fe_3O_4)_x$ (date not shown),

Preprints (www.preprints.org) | NOT PEER-REVIEWED | Posted: 23 October 2020 doi:10.20944/preprints202010.0498.v1

implying that heterosphere diffusion reaction may be some role in the adsorption process [8,9].

Table 4 Adsorption kinetic model parameters

Adsorbate	Pseudo-first-order kinetic			Pseudo-second-order kinetic		
	q_e/(mg/g)	k_1/(min^{-1})	R^2	q_e/(mg/g)	k_2/(g/(mg·min))	R^2
Sb(III)	32.575	0.018	0.945	37.845	0.001	0.985
Sb(V)	39.810	0.018	0.923	44.029	0.001	0.982

3.6 Desorption

The repeated adsorption/desorption test of HCO-doped-$(Fe_3O_4)_x$ was conducted with 0.2 mol/L NaOH solution as desorption agent. As shown in Table 5, HCO-doped-$(Fe_3O_4)_x$ maintained a good removal performance for Sb(III) and Sb(V) (86.55% and 71.33%) after 3 cycle, reflecting its high stability and good regeneration performance. The main reason is that there is competition adsorption between OH^- ions and Sb(III) and Sb(V) ion on the surface of HCO-doped-$(Fe_3O_4)_x$ [8]. This performance lays a good foundation for the reuse of HCO-doped-$(Fe_3O_4)_x$ adsorbent and the recycling of Sb, and has a good economic value.

Table.5 Variation of removal rate of HCO-doped-$(Fe_3O_4)_x$ adsorbent in adsorption/desorption process.

Removal rate (%)	Number of cycles					
	0	1	2	3	4	5
Sb(III)	98.17	94.25	90.37	86.55	74.68	62.78
Sb(V)	96.86	91.46	83.28	71.33	54.39	-

3.7 Adsorption mechanism

Based on the foregoing analysis, some possible adsorption mechanisms of Sb(III)/Sb(V) by HCO-doped-$(Fe_3O_4)_x$ could be summarized as follows:

(1) The Pseudo-second-order kinetic model fitted better for the adsorption of Sb(III) and Sb(V) onto HCO-doped-$(Fe_3O_4)_x$, and the adsorption process was controlled by the chemical reaction at the solid-liquid interface [4,14,28]. Furthermore, Langmuir model was suitable for describing the sorption behavior of Sb(III) by HCO-doped-$(Fe_3O_4)_{1.5}$, but Freundlich model was suitable for describing the sorption behavior of Sb(V) by HCO-doped-$(Fe_3O_4)_{1.0.}$ It could be concluded that there existed different adsorption pathway between the Sb(III) and Sb(V) onto HCO-doped-$(Fe_3O_4)_x$. Simultaneously, HCO-doped-$(Fe_3O_4)_x$ exhibited high surface area which could provide more adsorption sites and more uniform adsorption.

(2)The type of ligand exchange reaction played a major role in adsorption process of Sb(III)/Sb(V) ions. As shown in Fig. 5, with doping Fe_3O_4, the compound $FeCe_2O_4$ was produced (Eq.(6)), which hinted that more negatively charged groups, hydroxyl groups existed on the surface of the HCO-doped-$(Fe_3O_4)_x$ [8]. Afterwards, electron transfer, ion transfer and sharing may occur in the hydrolyzation process of of $FeCe_2O_4$, and forming

Preprints (www.preprints.org) | NOT PEER-REVIEWED | Posted: 23 October 2020 doi:10.20944/preprints202010.0498.v1

amorphous hydrated iron oxide X≡Fe-OH with a double electron layer structure [4,50], which could provide higher specific surface area and more hydroxyl groups. Furthermore, coordination body exchange reactions of the X≡Fe-OH with the Sb(III)/Sb(V) ions, may result in complex compounds containing antimony, such as $FeOH_2SbO_3$ (Eq. (14)), $X≡Fe\text{-}Sb(OH)_2$ (Eq. (15)), $FeOSb(OH)_6$ (Eq. (18)) and $Fe\text{-}O\text{-}Sb(OH)_5^-$ (Eq. (19)) [4,14], and had been identified by the XRD results. Therefore, the adsorption capacity and Sb(III)/Sb(V) adsorption performance was improved remarkably.

(3) Complexation and oxidation reactions also were favorable for adsorption of antimony. As shown in Fig. 2(a) and Fig. 2(c, e), it could be concluded that Ce element in HCO-doped-$(Fe_3O_4)_x$ was mainly in the form of CeO_2 and Ce_2O_3 [4,14]. The peak binding energy of Ce(III) shifted after adsorption of Sb(III)/Sb(V), and indicated that Ce_2O_3 reacted with Sb(III) or Sb(V) to generate Ce-O-Sb compounds in the form of $CeSbO_3$(Eq. (12)) or $CeSbO_4$(Eq. (17)) [4]. The results of Fig.2(f) showed that a prominent peak appeared at the binding energy of 531.68ev, indicating the existence of Sb(V) valence state [28], meanwhile, both of the peak binding energy of Ce and Fe shifted (Fig. 2(c) and Fig. 2(e)). Considering the oxidizing ability of CeO_2 [51, 52], it was inferred that Sb(III) could be oxidized to Sb(V) by CeO_2 and Fe_2O_3 during the adsorption process, to form Ce-O-Sb and Fe-O-Sb complexes [4,28], and then Sb(V) was removed by the reaction of formulas (Eq.18-19). In addition, there no Sb(III) absorption peak appeared after Sb(V) adsorption, stating clearly no reduction reaction occurred in this process.

$$Ce_2O_3 + 2Sb(OH)_3 \rightarrow 2CeSbO_3 + 3H_2O \quad (12)$$

$$2Ce^{4+} + Sb^{3+} \rightarrow 2Ce^{3+} + Sb^{5+} \quad (13)$$

$$FeOOH + SbO_3^{3-} + H^+ \rightarrow FeOH_2SbO_3 + H_2O \quad (14)$$

$$X≡Fe-OH + Sb(OH)_3 \rightarrow X≡Fe\text{-}Sb(OH)_2 + H_2O \quad (15)$$

$$FeO\cdot Fe_2O_3 + Sb^{3+} + 2H^+ \rightarrow Sb^{5+} + 3FeO + H_2O \quad (16)$$

$$Ce_2O_3 + 2Sb(OH)_6^- + 2H^+ \rightarrow 2CeSbO_4 + 7H_2O \quad (17)$$

$$FeOOH + Sb(OH)_6^- + H^+ \rightarrow FeOSb(OH)_6 + H_2O \quad (18)$$

$$X≡Fe\text{-}OH + Sb(OH)_6^- \rightarrow Fe\text{-}O\text{-}Sb(OH)_5^- + H_2O \quad (19)$$

In conclusion, the mechanism of HCO-doped-$(Fe_3O_4)_x$ adsorbing Sb(III)/Sb(V) mainly includes ligand exchange reaction and complexation reaction on the surface of adsorbent. In addition, Sb(III) can be oxidized to Sb(V) by reaction with CeO_2 and Fe_2O_3, which is why there is a difference between the adsorption of Sb(III) and Sb(V) by HCO-doped-$(Fe_3O_4)_x$ adsorbent.

Preprints (www.preprints.org) | NOT PEER-REVIEWED | Posted: 23 October 2020 doi:10.20944/preprints202010.0498.v1

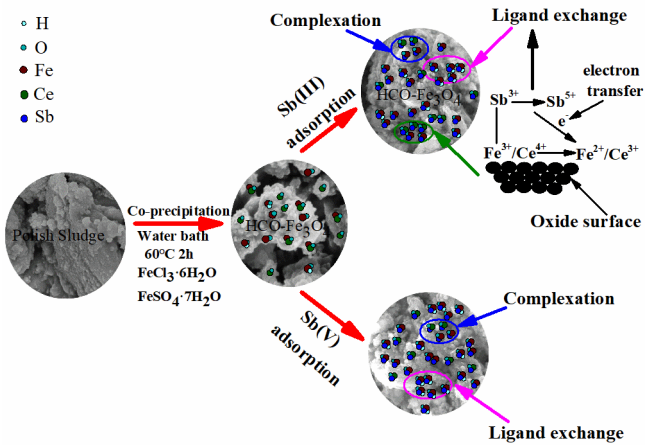

Fig. 5 Formation process of HCO-doped-$(Fe_3O_4)_x$ adsorbent and the adsorption mechanism for Sb(III) and Sb(V)

4 Conclusions

In summary, this study prepared HCO-doped-$(Fe_3O_4)_x$ adsorbent from a modified co-precipitation method, by which Fe_3O_4 was doped with HCO sludge matrix, and then applied as an effective adsorbent for aqueous removal of Sb(III)/Sb(V) ions. According to the results of EDS, XPS and XRD measurements, it was shown that Fe_3O_4 was successfully doped into HCO sludge. The calculated maximum adsorption capacity for Sb(III) onto HCO-doped-$(Fe_3O_4)_{1.5}$ was 44.46 mg/g at the pH of 3.0. Meanwhile, the calculated maximum adsorption capacity for Sb(V) onto HCO-doped-$(Fe_3O_4)_{1.0}$ was 47.91 mg/g at the pH of 2.0. The optimum efficiency for removal for Sb(III) was found to be when Fe mol fraction was 0.4 but optimum removal for Sb(v) was when Iron mol fraction was 0.5 within the HCO-doped-$(Fe_3O_4)_x$ Iron complex. The adsorption kinetics followed the pseudo-second-order kinetic model which stated clearly adsorption process of Sb(III)/Sb(V) by HCO-doped-$(Fe_3O_4)_x$ adsorbent was controlled mainly by chemical reaction. The main adsorption mechanism is that antimony ion and amorphous iron oxide X≡Fe-OH undergo coordination exchange reaction and complexation reaction with CeO_2 or Ce_2O_3. Sb(III) could be oxidized by CeO_2 and Fe_3O_4 to Sb(V) resulting in lower removal rate of the latter. Moreover, the HCO-doped-$(Fe_3O_4)_x$ adsorbent could be readily regenerated using 0.1mol/L NaOH solution and be repeatedly used. HCO-doped-$(Fe_3O_4)_x$ adsorbent can adsorb Sb(III)/Sb(V) with high adsorption capacity and adsorption speed can be used as a promising adsorbent to remove antimony from aqueous solution.

Acknowledgments

This study was financially supported by the National Natural Science Foundation of China (No. 41672350, No.41702329) and the scientific research project of the Hunan Provincial Education Department (No.18A184, No.17B097). Andrew S. Hursthouse acknowledges the support of Hunan Provincial

Government and Hunan University of Science & Technology through the High End Expert Scholarship.

Reference

1. Ungureanu, G.; Santos, S.; Boaventura, R.; Botelho, C. Arsenic and antimony in water and wastewater: overview of removal techniques with special reference to latest advances in adsorption. *J Environ Manage.* **2015,** 151, 326-42.
2. Li, J.; Zheng, B.; He, Y.; Zhou, Y.; Chen, X.; Ruan, S.; Yang, Y.; Dai, C.; Tang, L. Antimony contamination, consequences and removal techniques: A review. *Ecotoxicol Environ Saf.* **2018,** 156, 125-134.
3. Smeets, J.; Amavis, R. European-Communities Directive Relating to the Quality of Water Intended for Human Consumption. *Water Air Soil Poll.* **1981,** 15, (4), 483-502.
4. Qi, Z.; Joshi, T. P.; Liu, R.; Liu, H.; Qu, J. Synthesis of Ce(III)-doped Fe3O4 magnetic particles for efficient removal of antimony from aqueous solution. *J Hazard Mater.* **2017,** 329, 193-204.
5. Hu, X.; Kong, L.; He, M. Kinetics and mechanism of photopromoted oxidative dissolution of antimony trioxide. *Environ Sci Technol.* **2014,** 48, (24), 14266-72.
6. He, M.; Wang, X.; Wu, F.; Fu, Z. Antimony pollution in China. *The Science of the total environment.* **2012,** 421-422, (3), 41-50.
7. Fu, Z.; Wu, F.; Amarasiriwardena, D.; Mo, C.; Liu, B.; Zhu, J.; Deng, Q.; Liao, H. Antimony, arsenic and mercury in the aquatic environment and fish in a large antimony mining area in Hunan, China. *The Science of the total environment.* **2010,** 408, (16), 3403-10.
8. Deng, R.-J.; Shao, R.; Ren, B.-Z.; Hou, B.; Tang, Z.-E.; Hursthouse, A. Adsorption of Antimony(III) onto Fe(III)-TreatedHumus Sludge Adsorbent: Behaviorand Mechanism Insights. *Polish Journal of Environmental Studies.* **2019,** 28, (2), 577-586.
9. Deng, R.-J.; Jin, C.-S.; Ren, B.-Z.; Hou, B.-L.; Hursthouse, A. The Potential for the Treatment of Antimony-Containing Wastewater by Iron-Based Adsorbents. *Water.* **2017,** 9, (10), 794.
10. Mendil, D.; Bardak, H.; Tuzen, M.; Soylak, M. Selective speciation of inorganic antimony on tetraethylenepentamine bonded silica gel column and its determination by graphite furnace atomic absorption spectrometry. *Talanta.* **2013,** 107, 162-6.
11. Miao, Y.; Han, F.; Pan, B.; Niu, Y.; Nie, G.; Lv, L. Antimony(V) removal from water by hydrated ferric oxides supported by calcite sand and polymeric anion exchanger. *J Environ Sci (China).* **2014,** 26, (2), 307-14.
12. Filella, M.; Belzile, N.; Lett, M. C. Antimony in the environment: A review focused on natural waters. III. Microbiota relevant interactions. *Earth-Science Reviews.* **2007,** 80,

 doi:10.20944/preprints202010.0498.v1

(3-4), 195-217.

13. Sarı, A.; Şahinoğlu, G.; Tüzen, M. Antimony(III) Adsorption from Aqueous Solution Using Raw Perlite and Mn-Modified Perlite: Equilibrium, Thermodynamic, and Kinetic Studies. *Industrial & Engineering Chemistry Research.* **2012,** 51, (19), 6877-6886.
14. Zhang, J.; Deng, R. J.; Ren, B. Z.; Hou, B.; Hursthouse, A. Preparation of a novel Fe3O4/HCO composite adsorbent and the mechanism for the removal of antimony (III) from aqueous solution. *Sci Rep.* **2019,** 9, (1), 13021.
15. Mittal, V. K.; Bera, S.; Narasimhan, S. V.; Velmurugan, S. Adsorption behavior of antimony(III) oxyanions on magnetite surface in aqueous organic acid environment. *Applied Surface Science.* **2013,** 266, (2), 272-279.
16. Xu, W.; Wang, H.; Liu, R.; Zhao, X.; Qu, J. The mechanism of antimony(III) removal and its reactions on the surfaces of Fe-Mn binary oxide. *Journal of Colloid & Interface Science.* **2011,** 363, (1), 320-326 %\ 2019-12-28 19:33:00.
17. Xu, W.; Liu, R.; Qu, J.; Peng, R. The adsorption behaviors of Fe-Mn binary oxide towards Sb(V). *Acta Scientiae Circumstantiae.* **2012,** 32, (2), 270-275.
18. Hu, X. Study on the performance and mechanism of the removal of antimony from mine waste water by a new type of Fe-Cu binary oxide. Hunan University of Science and Technology, 2016.
19. Biswas, B. K.; Inoue, J.; Kawakita, H.; Ohto, K.; Inoue, K. Effective removal and recovery of antimony using metal-loaded saponified orange waste. *Journal of Hazardous Materials.* **2009,** 172, (2-3), 721-728.
20. Shi, S.; Yang, J.; Liang, S.; Li, M.; Gan, Q.; Xiao, K.; Hu, J. Enhanced Cr(VI) removal from acidic solutions using biochar modified by Fe3O4@SiO2-NH2 particles. *The Science of the total environment.* **2018,** 628-629, 499-508.
21. Yang, Q.; Wang, X.; Luo, W.; Sun, J.; Xu, Q.; Chen, F.; Zhao, J.; Wang, S.; Yao, F.; Wang, D.; Li, X.; Zeng, G. Effectiveness and mechanisms of phosphate adsorption on iron-modified biochars derived from waste activated sludge. *Bioresour Technol.* **2018,** 247, 537-544.
22. Chubar, N.; Gerda, V.; Banerjee, D. Influence of 300 °C thermal conversion of Fe-Ce hydrous oxides prepared by hydrothermal precipitation on the adsorptive performance of five anions: Insights from EXAFS/XANES, XRD and FTIR (companion paper). *Journal of Colloid and Interface Science.* **2017,** 491, 111-122.
23. Sun, J.; Zhang, X.; Zhang, A.; Liao, C. Preparation of Fe-Co based MOF-74 and its effective adsorption of arsenic from aqueous solution. *J Environ Sci (China).* **2019,** 80, 197-207.

24. Wang, T.; Yang, W.; Song, T.; Li, C.; Zhang, L.; Wang, H.; Chai, L. Cu doped Fe3 O4 magnetic adsorbent for arsenic: synthesis, property, and sorption application. *RSC Advances.* **2015,** 5, (62), 50011-50018.
25. Reddy, D. H. K.; Yun, Y.-S. Spinel ferrite magnetic adsorbents: Alternative future materials for water purification? *Coordination Chemistry Reviews.* **2016,** 315, 90-111.
26. Zhang, S. X.; Niu, H. Y.; Cai, Y. Q.; Zhao, X. L.; Shi, Y. L. Arsenite and arsenate adsorption on coprecipitated bimetal oxide magnetic nanomaterials: MnFe2O4 and CoFe2O4. *Chemical Engineering Journal.* **2010,** 158, (3), 599-607.
27. Zhang, Y.; Yang, M.; Dou, X. M.; He, H.; Wang, D. S. Arsenate adsorption on an Fe-Ce bimetal oxide adsorbent: Role of surface properties. *Environmental Science & Technology.* **2005,** 39, (18), 7246-7253.
28. Wang, L.; Wang, J. Y.; Wang, Z. X.; Feng, J. T.; Li, S. W.; Yan, W. Synthesis of Ce-doped magnetic biochar for effective Sb(V) removal: Performance and mechanism. *Powder Technology.* **2019,** 345, 501-508.
29. Wang, L.; Wang, J. Y.; Wang, Z. X.; He, C.; Lyu, W.; Yan, W.; Yang, L. Enhanced antimonate (Sb(V)) removal from aqueous solution by La-doped magnetic biochars. *Chemical Engineering Journal.* **2018,** 354, 623-632.
30. Son, E. B.; Poo, K. M.; Chang, J. S.; Chae, K. J. Heavy metal removal from aqueous solutions using engineered magnetic biochars derived from waste marine macro-algal biomass. *The Science of the total environment.* **2018,** 615, 161-168.
31. Chen, B.; Zhu, Z.; Guo, Y.; Qiu, Y.; Zhao, J. Facile synthesis of mesoporous Ce-Fe bimetal oxide and its enhanced adsorption of arsenate from aqueous solutions. *J Colloid Interface Sci.* **2013,** 398, 142-51.
32. Zhang, Y.; Dou, X. M.; Zhao, B.; Yang, M.; Takayama, T.; Kato, S. Removal of arsenic by a granular Fe-Ce oxide adsorbent: Fabrication conditions and performance. *Chemical Engineering Journal.* **2010,** 162, (1), 164-170.
33. Li, Y.; Geng, B.; Hu, X.; Ren, B.; Hursthouse, A. S. Preparation and characterization of iron-copper binary oxide and its effective removal of antimony(III) from aqueous solution. *Water Sci Technol.* **2016,** 74, (2), 393-401.
34. Xi, J. H.; He, M. C.; Lin, C. Y. Adsorption of antimony(III) and antimony(V) on bentonite: Kinetics, thermodynamics and anion competition. *Microchemical Journal.* **2011,** 97, (1), 85-91.
35. Fan, H. T.; Sun, W.; Jiang, B.; Wang, Q. J.; Li, D. W.; Huang, C. C.; Wang, K. J.; Zhang, Z. G.; Li, W. X. Adsorption of antimony(III) from aqueous solution by mercapto-functionalized silica-supported organic-inorganic hybrid sorbent: Mechanism

 doi:10.20944/preprints202010.0498.v1

insights. *Chemical Engineering Journal.* **2016,** 286, 128-138.

36. Chen, Y. Effects of lanthanum ions on the crystal structure and photocatalytic properties of cerium oxide. Chendu University of Technology, 2018.
37. Guo, X.; Wu, Z.; He, M.; Meng, X.; Jin, X.; Qiu, N.; Zhang, J. Adsorption of antimony onto iron oxyhydroxides: adsorption behavior and surface structure. *J Hazard Mater.* **2014,** 276, 339-45.
38. Kolbe, F.; Weiss, H.; Morgenstern, P.; Wennrich, R.; Lorenz, W.; Schurk, K.; Stanjek, H.; Daus, B. Sorption of aqueous antimony and arsenic species onto akaganeite. *Journal of Colloid and Interface Science.* **2011,** 357, (2), 460-465.
39. Filella, M.; Belzile, N.; Chen, Y. W. Antimony in the environment: a review focused on natural waters II. Relevant solution chemistry. *Earth-Science Reviews.* **2002,** 59, (1-4), 265-285.
40. Farquhar, M. L.; Charnock, J. M.; Livens, F. R.; Vaughan, D. J. Mechanisms of arsenic uptake from aqueous solution by interaction with goethite, lepidocrocite, mackinawite, and pyrite: an X-ray absorption spectroscopy study. *Environ Sci Technol.* **2002,** 36, (8), 1757-62.
41. Hayes, K. F.; Leckie, J. O. Modeling Ionic-Strength Effects on Cation Adsorption at Hydrous Oxide-Solution Interfaces. *Journal of Colloid and Interface Science.* **1987,** 115, (2), 564-572.
42. Chmielewska, E.; Tylus, W.; Drabik, M.; Majzlan, J.; Kravcak, J.; Williams, C.; Caplovicova, M.; Caplovic, L. Structure investigation of nano-FeO(OH) modified clinoptilolite tuff for antimony removal. *Micropor Mesopor Mat.* **2017,** 248, 222-233.
43. Shan, C.; Ma, Z.; Tong, M. Efficient removal of trace antimony(III) through adsorption by hematite modified magnetic nanoparticles. *J Hazard Mater.* **2014,** 268, 229-36.
44. Li, X.; Dou, X.; Li, J. Antimony(V) removal from water by iron-zirconium bimetal oxide: performance and mechanism. *J Environ Sci (China).* **2012,** 24, (7), 1197-203.
45. Wang, L.; Wan, C.; Lee, D. J.; Liu, X.; Zhang, Y.; Chen, X. F.; Tay, J. H. Biosorption of antimony(V) onto Fe(III)-treated aerobic granules. *Bioresource Technology.* **2014,** 158, (2), 351-354.
46. Verbinnen, B.; Block, C.; Lievens, P.; Van Brecht, A.; Vandecasteele, C. Simultaneous Removal of Molybdenum, Antimony and Selenium Oxyanions from Wastewater by Adsorption on Supported Magnetite. *Waste Biomass Valori.* **2013,** 4, (3), 635-645.
47. Anirudhan, T. S.; Suchithra, P. S.; Radhakrishnan, P. G. Synthesis and characterization of humic acid immobilized-polymer/bentonite composites and their ability to adsorb basic dyes from aqueous solutions. *Applied Clay Science.* **2009,** 43, (3-4), 336-342.

48. Rooygar, A. A.; Mallah, M. H.; Abolghasemi, H.; Safdari, J. New "Magmolecular" Process for the Separation of Antimony(III) from Aqueous Solution. *J Chem Eng Data.* **2014,** 59, (11), 3545-3554.
49. Wan, C. L.; Wang, L.; Lee, D. J.; Zhang, Q. L.; Li, J. N.; Liu, X. Fungi aerobic granules and use of Fe(III)-treated granules for biosorption of antimony(V). *Journal of the Taiwan Institute of Chemical Engineers.* **2014,** 45, (5), 2610-2614.
50. Sheng, T. Adsorption activity of low concentration arsenic on amended honeycomb cinder/Fe3O4 composite. Zhe Jiang University, 2014.
51. HE, L.; LIAO, Y.; CHEN, L.; FU, M.; WU, J.; HUANG, B.; YE, D. Shape effect of ceria nanocrystals with various morphologies on toluene catalytic oxidation. *Acta Scientiae Circumstantiae.* **2013,** 33, (9), 2412-2421 %\ 2019-12-28 19:35:00.
52. Basu, T.; Nandi, D.; Sen, P.; Ghosh, U. C. Equilibrium modeling of As(III,V) sorption in the absence/presence of some groundwater occurring ions by iron(III)-cerium(IV) oxide nanoparticle agglomerates: A mechanistic approach of surface interaction. *Chemical Engineering Journal.* **2013,** 228, 665-678.